Article

Not peer-reviewed version

Comparison between nano-Hydroxyapatite/ Beta-Tricalcium Phosphate Composite and Autogenous Bone Graft in Bone Regeneration Applications: Biochemical Mechanisms and Morphological Analysis

Igor da silva Brum *, Lucio Frigo, Jemima Fuentes Ribeiro da Silva, Bianca Torres Ciambarella, Ana Lúcia Rosa Do Nascimento, Mario José dos Santos Pereira, Carlos Nelson Elias, Jorge José de Carvalho

Posted Date: 24 October 2024

doi: 10.20944/preprints202410.1932.v1

Keywords: bone graft; autogenous bone; biomaterial; hydroxyapatite; beta-tricalcium phosphate

Article

Comparison between nano-Hydroxyapatite/ Beta-Tricalcium Phosphate Composite and Autogenous Bone Graft in Bone Regeneration Applications: Biochemical Mechanisms and Morphological Analysis

Igor da Silva Brum [1,*], Lucio Frigo [2], Jemima Fuentes Ribeiro da Silva [3], Bianca Torres Ciambarella [3], Ana Lucia Rosa Nascimento [3], Mario José dos Santos Pereira [1], Carlos Nelson Elias [4] and Jorge José de Carvalho [5]

[1] Department of Implantology, School of Dentistry, State University of Rio de Janeiro. 157, 28 de setembro, Boulevard, Rio de Janeiro, Brazil. P.O. box 20551-030.
[2] Department of Basic Sciences, Faculdade de Odontologia da Associação Paulista de Cirurgiões Dentistas. 457, Voluntarios da Patria, St. São Paulo, 02011-000, Brazil.
[3] Laboratory of Ultrastructure and Tissue Biology, Department of Histology and Embryology, State University of Rio de Janeiro, Rio de Janeiro, 20550-900, Brazil.
[4] Instituto Militar de Engenharia. 80, Praça Gen. Tiburcio, Rio de Janeiro, 22290-270, Brazil.
[5] Department of Biology, School of Medicine, State University of Rio de Janeiro. 444, Professor Manuel de Abreu, Avenue, Rio de Janeiro, 20550-170, Brazil.
* Correspondence: igor_brum1@hotmail.com

Abstract: It was assumed that only autogenous bone had appropriate osteoconductive and osteoindutive properties for bone regeneration, but this assumption has been challenged. Many studies have shown that synthetic biomaterials must be considered as the best choice for bone guided regeneration. The objective of this work is to compare the performances of nano-hydroxyapatite/β-Tricalcium phosphate (n-HA/β-TCP) composite and autogenous bone graft in bone regeneration applications. Th composite was characterized by scanning electron microscopy (SEM) and used as an allograft in bone defects made in adult Wistar rats. The bone defects in the dorsal cranium were grafted with autogenous bone on one side and the n-HA/β-TCP composite on the other. Histomorphometry evaluation by different staining methods (Goldner trichrome, PAS, Sirius red) and TRAP histochemistry were performed. The immunohistomorphometries to OPN, Cathepsin-K, TRAP, Acid phosphatase, VEGF, NFκ-β, MMP-2, MMP-9, and TGF-β were carried out. The RT-PCR method to *RANK-L, Osteocalcine, Alcaline Phosphatase, Osterix,* and *Runx2* were conducted as well. The results showed that all morphometric evaluations on the different staining methods, histochemistry and immunohistochemistry, VEGF and NFκ-β, were higher on the n-HA/β-TCP composite group than in the autogenous bone graft group. The RT-PCR markers were higher in the autogenous bone group than on the n-HA/β-TCP composite group. The n-HA/β-TCP composite exhibited enhanced cell-matrix interactions in bone remodeling, higher adhesion, proliferation, and differentiation, and increased vascularization. These results suggests that the n-HA/β-TCP composite induces faster bone formation than autogenous bone.

Keywords: bone graft; autogenous bone; biomaterial; hydroxyapatite; beta-tricalcium phosphate

1. Introduction

The research and development of biomaterials have been pressed to design new products and to improve the ones already available due the growing demand for bone grafts and substitutes. Bone grafts and substitutes are used in surgical procedures when a bone fracture occurs or when there is bone loss. Bone loss and reduced bone density occur due to factors such as old age and degenerative diseases. The literature estimates that 2.2 million of clinical procedures involving bone grafts are

 doi:10.20944/preprints202410.1932.v1

annually registered. [1] The market size for global bone grafts and substitutes was valued at2.80 billion dollars in 2022, and an expected annual growth rate of 6.2% up to 2030 is expected. [2] The increased demand is related to severe bone injury and bone loss increase due to trauma, tumor, infections, surgical resections and some age-related diseases. [3]

Some authors stated that the ideal biomaterial for bone grafts should exhibit the following biological properties: (1) biocompatibility: the biomaterial and its metabolites should be nontoxic; (2) biodegradability: it should be completely absorbable after achieving its goals; (3) bioplasticity: it should adopt the desired shape and respond to the mechanical demands of the tissue; (4) osteoinductivity: it should provide differentiation of mesenchymal stem cells to osteoprogenitor cells and promote bone formation at heterotopic places; (5) osteoconductivity: it should provide a 3D scaffold able to support blood vessel sprouting and osteoprogenitor cells anchoring to new bone formation; (6) sterilizable: it should be suitable to common sterilization procedures without reducing its biological properties. [4–6]

The search/design of the ideal biomaterial ought to be preceded by a comprehensive understanding of bone formation, remodeling and healing mechanisms. Detailed and extensive descriptions of bone physiology provide a solid background to biomaterial design and/or evaluation. [7–9]

Bone healing is a regenerative process. The mechanism starts with formation of a new bone tissue and, subsequently, its remodeling. The process is based on cell migration, differentiation, extracellular matrix production and mineralization. [10,11]

Clot formation after bone injury and the inflammation process that follows, are responsible for the release of a myriad of cell mediators related to cell migration and differentiation. [12] Bone morphogenic protein 4 (BMP4), interleukine-6 (IL-6), vascular endothelial growth factor (VEGF), platelet-derived growth factor (PDGF), and transforming growth factor-β (TGF-β) are important mediators in the process. The mediators induce the recruitment of mesenchymal stem cells (MSCs), commitment to osteoprogenitor cell line, osteoblast differentiation, osteoclast precursor recruitment and vascular sprouting. [13–19]

In the intracellular level, Runx2 (Runt-related transcription factor 2), SOX9 and Osterix (OSX) gene expression mark the commitment to mature osteoblasts. The nuclear factor κB (NFκB), c-fos, TNF (tumor necrosis factor) receptor-associated factor 6 (TRAF6). and sequestosome 1 (SQSTM1) are transcription factors required for osteoclast differentiation. The release of notch intracellular domain (NCID) by γ-secretase complex and presenilin 1 (PS1) or PS2 is linked to type H endothelial cells in the revascularization site. [20–25]

The first report of biomaterial development (synthetic calcium phosphate) dates back to the 30's. In the 60's and 70's biopolymers and bioglasses were designed and in 1985 the description of the BMPs further propelled biomaterials design. In 1990 and 2000 witnessed the union of calcium phosphate with peptides and different types of materials. However, for more than a decade, hydroxyapatite was in evidence, until the appearance of the hydroxyapatite/β-TCP composite. More recently, nanotechnology has enhanced the osteoinductive and osteoconductive properties of the biomaterials. [26] (Figure 1)

 doi:10.20944/preprints202410.1932.v1

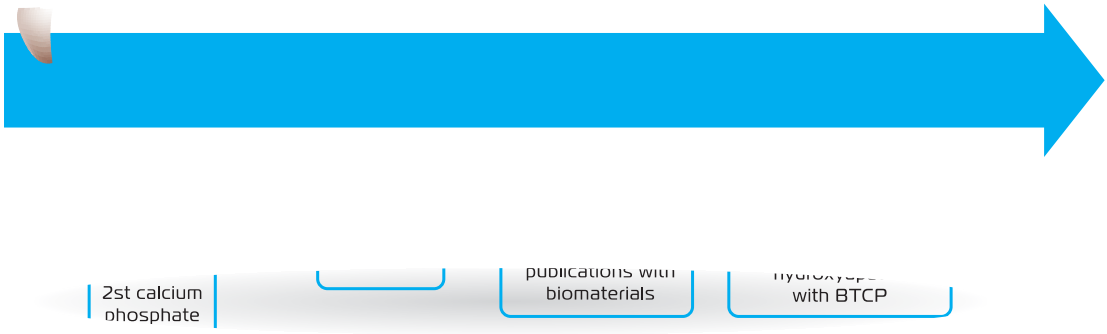

Figure 1. Timeline of the main events related to biomaterial design/research.

In case of extensive bone loss. a bone graft is usually used to fill the defect and guide new bone formation (osteoconduction). According to the source, bone grafts can be classified as: (1) autograft: the donor and receptor are the same individual, (2) isograft: the donor is an identical twin, (3) allograft: the donor is from the same species, (4) xenograft: the donor is from a different species and (5) synthetic: biomaterials similar to bone are used. [27,28] Autogenous bone is considered the "golden standard" due to is potential to trigger osteoinduction and osteoconduction. However, autogenous bone graft has limitations related to the extension of bone loss and morbidity in the site from where the bone is extracted. [29,30] **N**anotechnology has stimulated a search for a synthetic biomaterial that could rival osteoinduction and osteoconduction of autogenous graft.

The aim of this work was to compare the osteoinduction performane of n-HA/β-TCP composite and autogenous bone use as grafts in critical bone defects in rats.

2. Material and Methods

Twelve adults male *Wistar* rats, 200-220 g of weight, provided by the Roberto Alcantara Biology Institute of Rio de Janeiro State University, were used. Animals were kept in individual cages with *ad libitum* access to food and water. Light/dark cycle (lights on at 7:00 AM, off at 7:00 PM) and temperature (22 °C) were kept constant. Experimental animal procedures protocol was approved by local Animal Ethics Committee (#001/2019).

The rats were anesthetized with ketamine hydrochloride/xilasine solution (1/1, 0,1mg/kg, i.p.). The dorsal cranium was trichotomized and a sagittal incision was carried out, using a sterile surgical scalp. Skin and periosteum were cleared in bilateral parietal region to prepare the bone defect. The bone defect was made using a sterilized punch (cutting edge Ø 3mm). The bone fragments were carefully removed to avoid damage of the duramater and related blood vessels. After biomaterial insertion in the bone defect, the skin was carefully replaced and cotton-wire sutured.

The rats were distributed into 2 groups:

Group 1: (n = 6): the bone defects were filled with 0,1g of calvarias autogenous bone.

Group 2: (n = 6): the bone defects were filled with 0,1g of the n-HA/ß-TCP composite.

Sixty days after surgery, the animals were euthanized under deep anesthesia, using ketamine hydrochloride/xilasine solution (1/1, 0,3mg/kg, i.p.). The animals were decapitated, and the heads sent to histological procedures.

 doi:10.20944/preprints202410.1932.v1

2.1. X-Ray Diffraction

X-ray diffraction (XRD) was used to analyze the n-HA/ß-TCP composite. A Panalytical Empyrean (Almelo, Netherlands) diffractometer was used, with Cu-Kα radiation, 2θ range of 20°–80°, a step width of 0.02°, and 5 s of exposure time. Identification of the diffraction peaks was based on comparison with IDCC (International Center for Diffraction Data) diffraction files and COD-Jan2012 (Crystallography en Database) PDF2-2004 databases. XRD data were analyzed by the Rietveld method to identify and quantify the phase percentage.

2.2. Morphological Analysis Protocol

The animal heads were trimmed and decalcified in EDTA (7.0%) in PBS (0.1M, pH 7.4) for 40 days. The specimens were washed in distilled water, dehydrated in alcohol (70, 95, 100%), clarified in dimetilbenzene and embedded in paraphin (Paraplast, Sigma-Aldrich, St. Louis, MO, USA) at 65°C. Serial sections of 7 μm thickness were cut, using a microtome (LEICA, Nussloch, Germany), and collected in silanized slides.

Histomorphometry evaluation was performed using three staining methods (Goldner trichrome, PAS, Sirius red) and TRAP histochemistry.

Slides were deparaffinized in xylene and rehydrated with alcohol (100, 95, 70%), washed in distilled water and immersed in Weigert's iron hematoxylin (Sigma-Aldrich, St. Louis, MO, USA) for 10 min. After washing in distilled water, slides were immersed in a Biebrich scarlet-acid fuchsin solution (Sigma-Aldrich, St. Louis, MO, USA) for 15 min, washed again with distilled water and immersed in a phosphomolybdic-phosphotungstic acid solution for 10 min. Aniline blue solution immersion for 5 min followed, washed again with distilled water, dehydrated and coverlipsed.

Slides were deparaffinized and rehydrated through alcohol (100, 95, 70%), washed in distilled water and immersed in periodic acid (1%) for 5 min and rinsed in distilled water. Slides were immersed in Schiff's reagent [Fuchsin Basic (1%), Sodium metabisulphite (2%) in HCl (2%) solution] for 5-15 min, followed by Wash in running tap water for 5-10 min, and counter stained with Herri's hematoxylin for 15 sec.

The slides were deparaffinized and bathed in acid phosphatase Burstone solution. Burstone solution was a mixture of naphthol AS-BI phosphate substrate (Sigma-Aldrich, St. Louis, MO, USA) (4mg) diluted in 0,25 ml de N–dimetil-formamida (Sigma-Aldrich, St. Louis, MO, USA) and 25 ml of acetate buffer (0,2M pH 5,0), 35mg of "Fast Red Violet" LB Salt (Sigma-Aldrich, St. Louis, MO, USA), and 2 drops de MgCl (10%). Followed a slide bath for 3h in D(-) tartaric acid (0,2352g) (Sigma-Aldrich, St. Louis, MO, USA). After bath, slides were rinsed in tap water, counter-stained with Harris hematoxilin (10%), clarified in xilol and coverlipsed in Entellan (EMS, Hatfield, PA, EUA)

Histological slides were initially deparaffinized in xylol baths (3 × 5 min) and hydrated in decreasing concentrations of alcohol (100%, 90%, 70%) for 5 min in each bath. were incubated in 3% hydrogen peroxide solution for 15 min in the dark, to inhibit endogenous peroxidase. After the inhibition of endogenous peroxidase activity, rinsing in PBS buffer at pH 7.2 was performed (3 × 5 min).

Antigenic site re-exposure was conducted in citrate buffer solution (pH 6.0 at 96 °C, for 20 min). After the slides cooled and were rinsed with a PBS buffer at pH 7.2 (3 × 5 min), nonspecific sites were blocked with PBS/BSA solution (3% for 20 min). After the rinsing, slides were incubated with the primary anti-VEGF antibody (Santa Cruz, sc-1876), diluted in PBS/BSA 1% (1:100) and primary anti-OPN, anti-CAL, anti-TRAP, anti-acid phosphatase, anti-VEGF, anti-TNF-alfa, anti-BMP-2, anti-BMP-9, anti-TGF-B antibody (Santa Cruz, sc-21742), and diluted in PBS/BSA 1% (1:200) overnight in a refrigerator (4.0 °C) in a humid chamber. After primary antibody incubation, 3 baths in PBS buffer solution at pH 7.2 (5 min) were carried out, followed by secondary biotinylated antibody (VECTASTAIN Universal Quick HRP Kit, Ingold Road, Burlingame, CA, USA) incubation for 1 h at room temperature.-After another PBS buffer solution rinse, slides were incubated with streptavidin (VECTASTAIN Universal Quick HRP Kit) for 30 min at room temperature. The streptavidin–biotin–peroxidase complex was revealed with diaminobenzidine (DAB) (VECTASTAIN Universal Quick HRP Kit). Slides were counterstained with hematoxylin solution (0.15%), dehydrated in increased

 doi:10.20944/preprints202410.1932.v1

alcohol concentrations (70%, 90%, 100%) (ethanol), diaphanized and mounted using Entellan resin (Sigma-Aldrich, St. Louis, MO, USA)

2.3. Image Acquisition and Histomorphometry

Slices stained with Goldner-Masson Trichrome, Periodic Acid Schiff or Immunostained were observed under a light microscope equipped with a CCD camera (Olympus BX53 with camera Olympus DP72, Nagano, Chubu, Japan) at 400X magnification. The quantification of each stain (three random fields) was performed with Image-Pro Plus 7.0 program (Media Cybernetics, Silver Springs, Maryland, EUA) (Figure 2). Graph Pad é programa estatístico (já está descirto no tópico análise estatística.

Three randomized slide fields in Goldner trichrome, PAS-stained and immune-labeled were photographed in photomicroscope (Carl Zeiss - JVC TK-1270 color video camera) in 200X magnifications. The images were quantified using GraphPad Prism Version 8.0. (Figure 2)

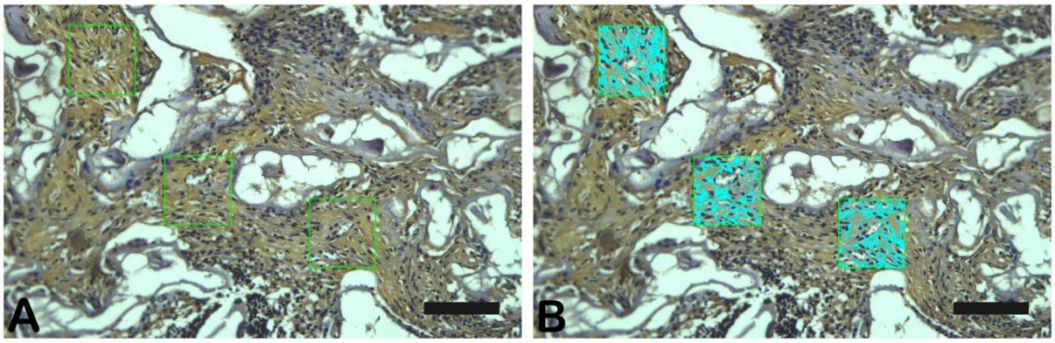

Figure 2. - Photomicrograph of TGF-β immunostaining as an example of data collection. Scale bar 100 μm, x200 magnification.

2.4RNA Isolation, Reverse Transcription, and Quantitative Real-Time PCR (qRT-PCR) Analysis

The frontal bone of 6 rats per group was removed, imbibed in RNA later Stabilization Solution (Invitrogen, Cat. AM7021, Carlsbad, CA, USA) and frozen in -80ºC until analysis. To isolate and purify the total RNA, the PureLink RNA Mini Kit (Invitrogen, Cat. 12183018A, Carlsbad, CA, USA) was used as datasheet information. The total RNA was quantified by Qubit using Quant It Kit RNA (Invitrogen, Cat. Q32852, Carlsbad, CA, USA) followed by DNAse treatment and a new total RNA quantification. To reverse transcriptase, a concentration of 500 ng/mL of total RNA was used and submit to SuperScript III First-Strand Synthesis System with Oligo dT prime (Invitrogen, Cat. 18080051, Carlsbad, CA, USA), in a cycle of 65ºC/5min; 50ºC/50min; 85ºC/5min; 37ºC/20min as described in datasheet. The cDNA product was diluted to final concentration of 50 ng/mL with RNAse free Water and 2 uL of this solution was used to qPCR. To amplification, the Forget-Me-Not, EvaGreen, qPCR Master Mix (Biotium, Cat. 31046, Fremont, CA, USA) was used in 1 cycle of 95ºC/2min followed by 40 cycles of 95ºC/5sec; 55ºC/10sec; 72ºC/20sec as described in datasheet.

The primers sequences are listed in table The dissociation melting curve was made as instrument guidelines and the result was expressed using β-actin as housekeeping gene and 2-DDCt to calculate the relative fold expression.

Table 1. – Primer's sequence.

Primer	**Forward**	**Reverse**
β-actin	5′-CAGAGCAAGAGAGGCATCCT-3′	5′-GTCATCTTTTCACGGTTGGC -3′
RANKL	5′-TCGCTCTGTTCCTGTACT-3′	5′-AGTGCTTCTGTGTCTTCG -3′
Osteocalcin	5′-CACAGGGAGGTGTGTGAG -3′	5′-TGTGCCGTCCATACTTTC-3′

 doi:10.20944/preprints202410.1932.v1

ALP	5′-GCCTGGACCTCATCAGCATT -3′	5′-GGGAAGGGTCAGTCAGGTTG -3′
Osterix	5′-GCCTACTTACCCGTCTGA-3′	5′-CTCCAGTTGCCCACTATT -3′
Runx2	5′-TAACGGTCTTCACAAATCCTC -3′	5′-GGCGGTCAGAGAACAAACTA-3′

2.5. ELISA Validation Test to Analysis of Acid Phosphatase (ap) Activity in Bone

The blood plasma and bone of 5 control animals were collected and used to compare the Acid Phosphatase activity. To extract AP of bone samples, we homogenized 6 to 10 mg of the bone tissue with 0.5 mL of lysis buffer (0.3M KCl, 0.1% Triton X-100). The samples were centrifuged at 20.744 rpm for 20 minutes at 4ºC and the supernatant was used for kit validation. The validation of the AP activity in bone samples was realized with Acid Phosphatase Colorimetric Assay Kit (# 10008051, Cayman Chemical/ Michigan, USA) and follows the datasheet method.

Briefly, 20 mL of each sample was added into a 96-wells plate with and without tartrate inhibitor followed by Acid Phosphatase substrate. The plate was incubated for 20 minutes at 37ºC followed by stop solution. The absorbance was measured at 405 nm and the AP activity was calculated as suggested in the kit datasheet.

2.6. Acid Phosphatase Assay

The bone samples were homogenized in 0.5 mL of lysis buffer (0.3M KCl, 0.1% Triton X-100). The samples were centrifuged at 20.744 rpm for 20 minutes at 4ºC and the supernatant was used to total protein quantification (Pierce™ BCA Protein Assay Kit, #23225, ThermoScientific / Carlsbad, USA) and AP assay (Acid Phosphatase Colorimetric Assay Kit, #10008051, Cayman Chemical/ Michigan, USA). About 7.6 mg of total protein were used to quantify the AP activity in the bone as described in the datasheet.

Each sample was added into the 96-wells plate with and without tartrate inhibitor followed by Acid Phosphatase substrate. The plate was incubated for 20 minutes at 37ºC followed by stop solution. The absorbance was measured at 405 nm and the AP activity was calculated as suggested in the kit datasheet.

Data were analyzed using one-way ANOVA, followed by a Kruskal-Wallis test ($p<0.05$). All Analysis was performed using the software's GraphPad Prism Version 8.0 and BioEstat 5.0.

2.7. Scanning Electron Microscopy

Immediately after euthanasia, samples were collected from the surgery sites. The samples were cut into small tissue blocks (1 mm^3), and fixed in 2.5% glutaldehyde in sodium cacodylate buffer (0,1M) at pH 7,4 at 4°C for 12h. After washes in 0.1 M sodium cacodylate buffer, fragments were postfixed with 1% osmium tetroxide diluted in 0.1 M sodium cacodylate buffer. After further washing, the material was dehydrated in an increasing series of ethanol (30%, 50%, 70%, 90% and 2x absolute), 30 min each step. The material was taken to the critical point device (Critical Point Dryer – CPD 030, Bal-Tec, Germany) for the replacement of ethanol by CO_2, later fixed in stubs with carbon tape and metallized with gold.

Before SEM analysis the samples were coated with gold film. An SEM Quanta 250 FEV (Thermo Fischer Scientific, USA) was used. Magnifications evaluated were: 5.000X to evaluate biomaterial homogeneity, 15.000X to evaluate cell clusters and architecture, 20.000X to evaluate specific cell types.

3. Results

3.1. X-Ray Diffraction

The diffraction pattern of the nano-HA/ß-TCP composite shows narrow, high, and well-defined peaks, which suggest an excellent crystallinity. (Figure 3).

 doi:10.20944/preprints202410.1932.v1

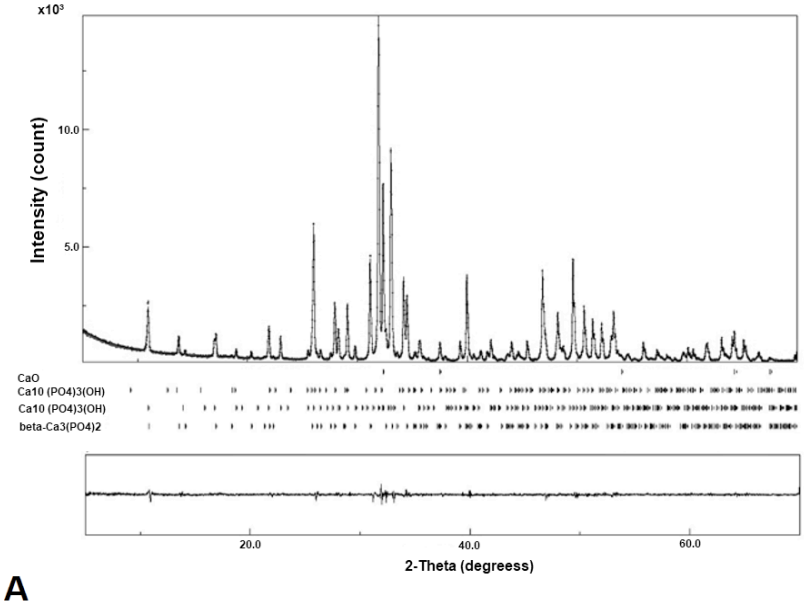

Figure 3. - Diffractogram of the n-HA/ß-TCP compound. (A).

The peaks (Figure 3) show the presence of three phases: β-$Ca_3(PO_4)_2$, with trigonal symmetry (Figure 4A), $Ca_{10}(PO_4)_3(OH)$, with hexagonal symmetry (Figure 4B), and $Ca_{10}(PO_4)_3(OH)$, with monoclinic symmetry (Figure 4C). The $Ca_{10}(PO_4)_3(OH)$ monoclinic phase has the highest concentration. The $Ca_{10}(PO_4)_3(OH)$ hexagonal phase appears only as a trace. This result indicates that the processing of the n-HA/ß-TCP compound induced the transformation of the hexagonal phase to monoclinic.

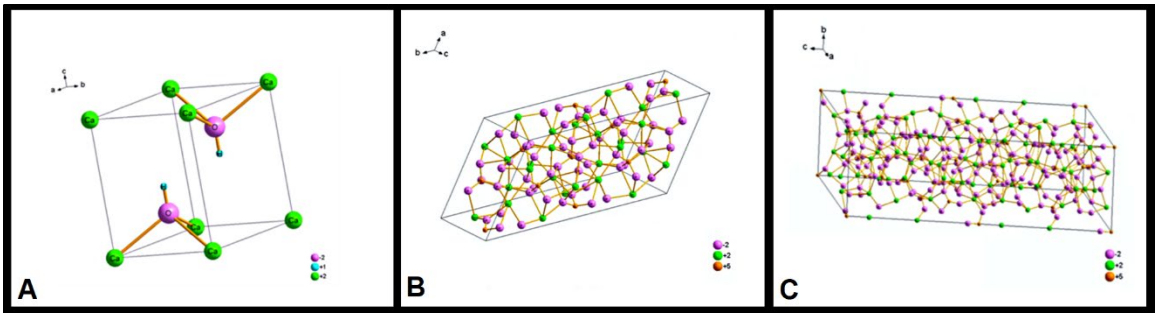

Figure 4. – Crystal structure of the n-HA/ß-TCP compound. (A) β-$Ca_3(PO_4)_2$ with trigonal symmetry. (B) $Ca_{10}(PO_4)_3(OH)$ with hexagonal symmetry. (C). $Ca_{10}(PO_4)_3(OH)$ with symmetry monoclinic.

3.2. Goldner's Trichromic Staining

The Goldner-Masson trichrome staining was applied to the regenerated bone structure. The critical defect treated with Blue Bone (B) was more suffused with newly formed bone than the Autogenous group (A) as seen by the increase in red areas in the image that indicate the osteoid bone matrix. Mineralized bone formation can be observed in green. (Figure 5)

 doi:10.20944/preprints202410.1932.v1

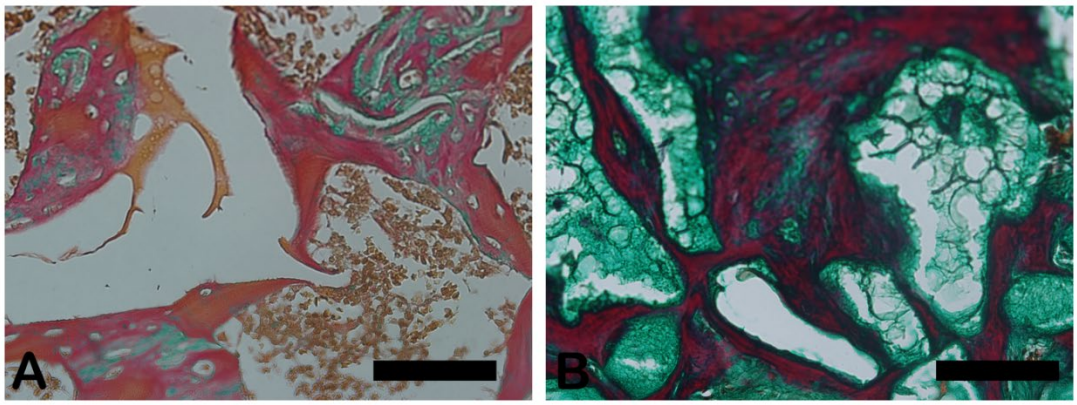

Figure 5. - Goldner's trichrome-stained slides photomicrographs. The osteoid bone matrix presents a red color and the bone matrix mature collagen can be observed in green: (**A**) Autogenous group, (**B**) Blue Bone group (REG). Scale bar 100 μm, ×200 magnification.

The red-stained osteoid matrix was more evident in the lining of the bone marrow, the blood vessels and the biomaterial. Group differences were related to the amount of red staining (Figure 6).

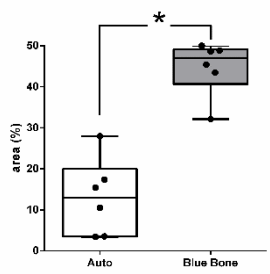

Figure 6. - Result of the histomorphometric analysis in the osteoid bone matrix bone areas stained by Goldner's trichrome method: Autogenous group and n-HA/ß-TCP compound * (p = 0,0022).

3.3. Picrosirius Red (PSR)

The picrosirius red slides indicates, in pink color, the collagenous osteoid bone matrix synthetized (Figure 7A) and the same microscopy field in polarized microscopy method. (Figure 7B). The Figure 8 shows the percentage of osteoid bone matrix bone and collagenous areas stained by Polarized picrosirius red.

The picrosirius red staining with polarized microscopic observation can be used to distinguish the maturation (thickness and packing) of type 1 collagen in the bone tissue. [31] Yellow and red stains represent mature type 1 collagen and green represents immature type 1 collage. The bone of calvaria (asterisk) exhibited a green color with areas of mature collagen (Yellow). In critical defects (star) higher immature collagen (green) content may be noted indicating bone regeneration.

 doi:10.20944/preprints202410.1932.v1

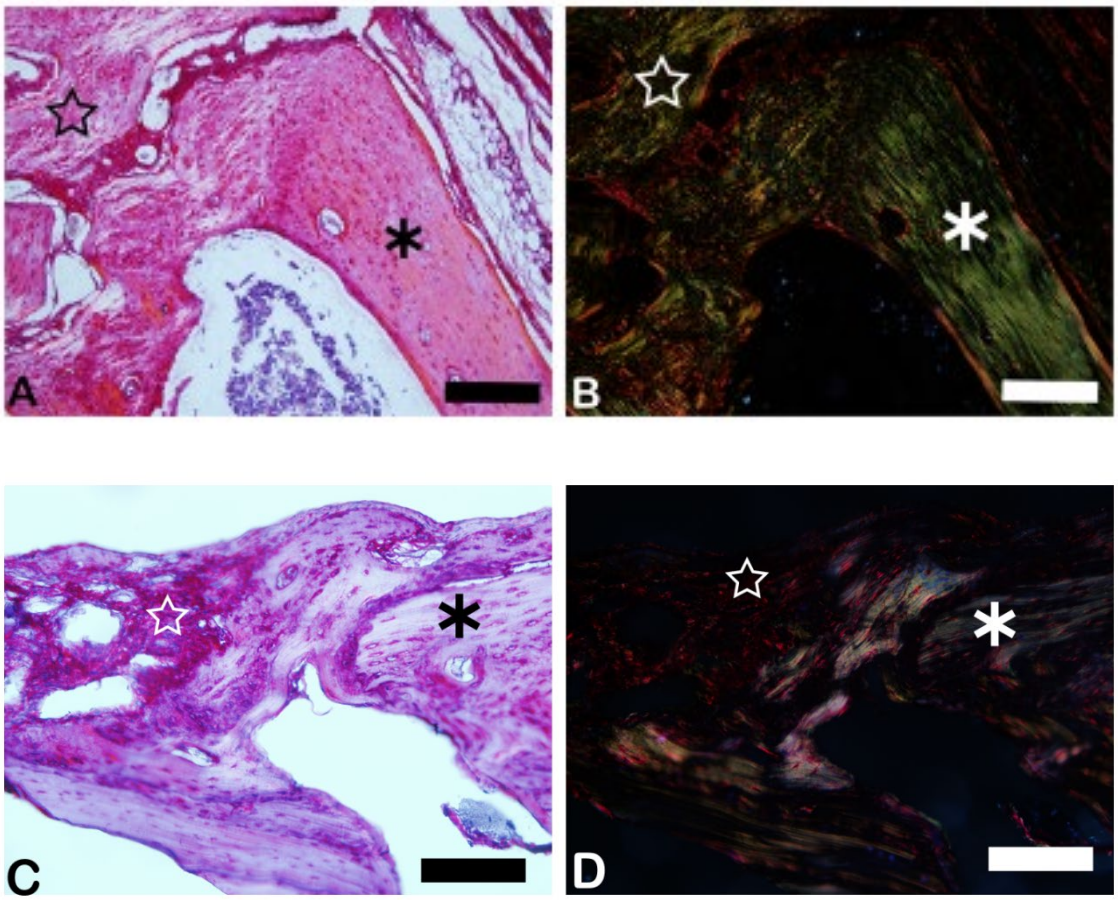

Figure 7. - Picrosirius-red stained sections observed under non-polarized (A), (C), and polarized light (B), (D), of the critical defects to detect collagen during bone remodeling. Polarized light can be used to distinguish the maturation (thickness and packing) of type 1 collagen in the bone tissue. Yellow and red stains represent mature type 1 collagen and green represents immature type 1 collagen. Bone calvaria (asterisk), critical defects (star). Scale bar 100 μm, ×200 magnification.

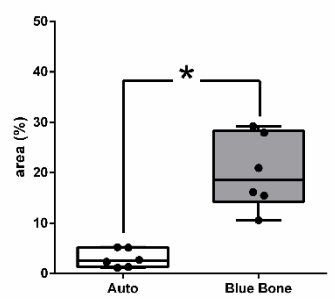

Figure 8. - Result of the histomorphometric analysis in the osteoid bone matrix bone and collagenous areas stained by-Picrosirius Red: Autogenous group and n-HA/β-TCP compound * p = 0.0022.

3.4. Cathepsin K

The Cathepsin K is an osteoclastic intracellular activity marker downstream to RANK-L and NFκ-β. Cathepsin K is responsible for the degradation of type I collagen in osteoclast-mediated bone resorption" – Referência: Wilson SR, Peters C, Saftig P, Brömme D. Cathepsin K activity-dependent regulation of osteoclast actin ring formation and bone resorption. J Biol Chem. 2009 Jan 23;284(4):2584-92. doi: 10.1074/jbc.MEpub 2008 Nov PMID: 19028686; PMCID: PMC2629117

 doi:10.20944/preprints202410.1932.v1

In Fig 8 the dark brown immunostained slide indicates Cathepsin K immunoreaction in autogenous graft (Figure 9A) and n-HA/β-TCP composite (Figure 9B). The Figure 10 shows the percentage of the osteoclast regulation through osteoblast activity by Cathepsin-K.

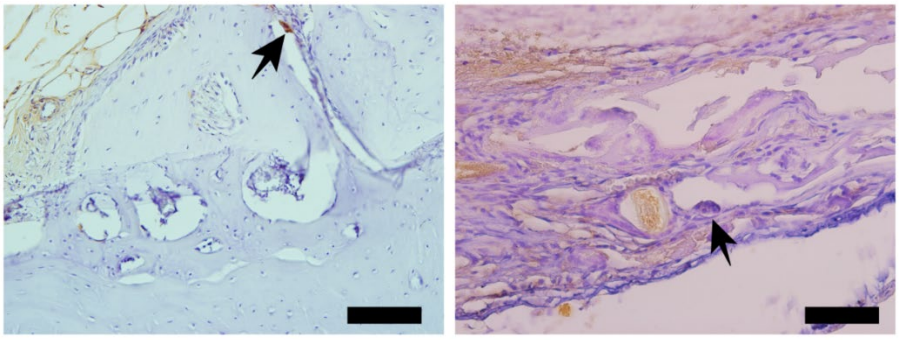

Figure 9. - Photomicrographs of Cathepsin K immunostaining (dark brown color) in autogenous bone (A) and n-HA/β-TCP composite (B). Scale bar 100 μm, x200 magnification.

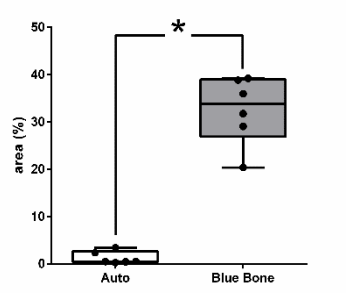

Figure 10. - Result of the histomorphometric analysis in the osteoclast regulation through osteoblast activity by Cathepsin-K: Autogenous bone group and n-HA/β-TCP composite group. * p = 0.0022.

3.5. Transforming Growth Factor-Beta (TGF-β)

The TGF-β induces osteoclasts apoptosis, blocking bone matrix reabsorption and osteoblasts recruitment. The dark brown immunostaining indicates TGF-β immunoreactivity in autogenous bone group (Figure 11A) and n-HA/β-TCP composite (Figure 11B). The Figure 12 shows the result of the histomorphometric analysis of immunostaining to TGF-β.

The TGF-B has a significant osteoinductive activity in vivo stimulating mesenchymal precursor cells to differentiate into osteoblasts and matrix formation. In the group B, was observed intense and diffuse staining in extracellular matrix being more intense in mesenchymal cells (asterisks) may suggest induction of new bone formation.

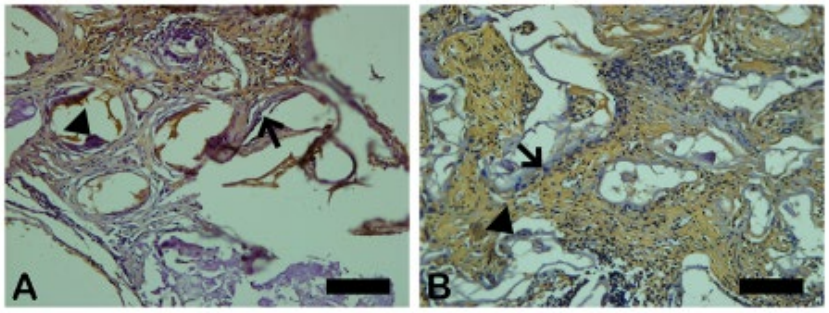

Figure 11. - Immunohistochemical labeling for TGF-B. (A) Moderate marking in osteoclasts (arrowhead), osteoblasts (arrow) and mesenchymal cells (asterisk). Slight staining of newly formed

 doi:10.20944/preprints202410.1932.v1

bone and intense staining appear in extracellular matrix (star). (B) Slight expression in osteoclasts (arrowhead), osteoblasts (arrow) and more intense in mesenchymal cells (asterisks). Intense and diffuse staining in extracellular matrix. Scale bar 100 μm, ×200 magnification.

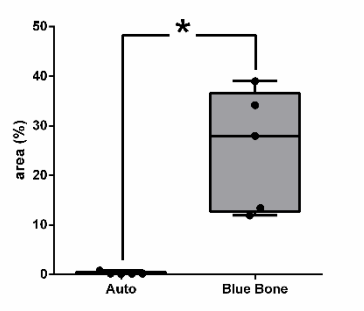

Figure 12. - Result of the histomorphometric analysis of immunostaining to TGF-β: Autogenous bone group and n-HA/β-TCP composite group. * p = 0.0079.

3.6. Osteopontin (OPN)

The Figure 13 shows the osteopontin-stained slides photomicrography. The slides showed dark brown deposits mostly found scattered in the decalcified bone matrix. Some round-nucleus cells (probably osteoblasts) presented high intensity deposits in cytoplasm. These round-nucleus-immunoreactive cells were found in higher numbers around biomaterials groups. The Figure 14 shows the area percentage of OPN in the samples. The stages of bone neoformation in the central region of the critical defects were evaluated through immunostaining for osteopontin (OP). OP it is a marker of immature bone tissue and was observed an extracellular matrix in the group B showing the beginning of the bone formation process.

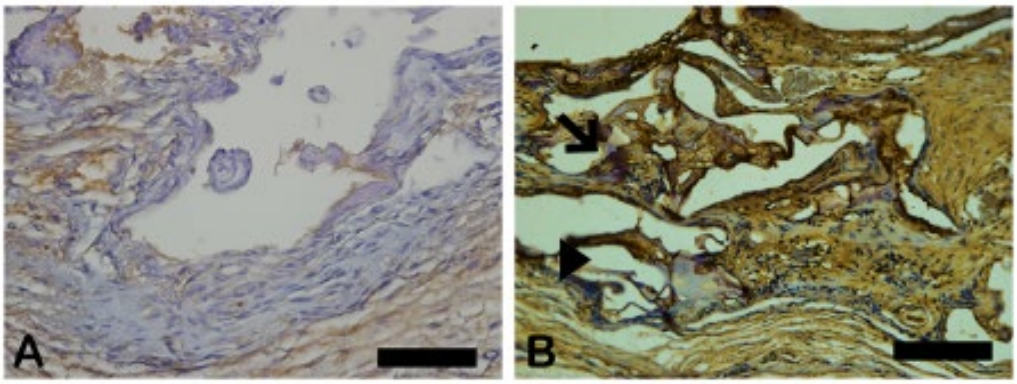

Figure 13. - Immunohistochemical labeling for OPN. (A) Extracellular OPN appeared to be very low in extracellular matrix (B) Intense and diffuse staining in extracellular matrix. Scale bar 100 μm, ×200 magnification**.**

In osteopontin-stained slides photomicrography, shades of brown indicate osteopontin deposits. Autogenous bone group (A) and n-HA/β-TCP composite group. * p = 0.Scale bar 100 μm, ×200 magnification.

 doi:10.20944/preprints202410.1932.v1

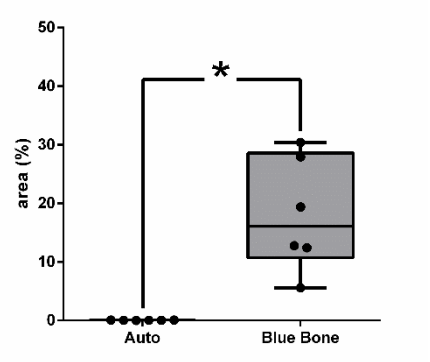

Figure 14. - Result of the histomorphometric analysis of immunostaining to OPN: Autogenous bone group and n-HA/β-TCP composite group. * p = 0.0022.

3.7. VEGF (Vascular Endothelial Growth Factor)

Vascular endothelial growth factor-immunoreactivity (VEGF) was observed mainly in cells cytoplasm close to and in the blood vessels in all tested groups. Only the n-HA/β-TCP composite group (Figure 15B) shows the presence of VEGF-ir. The VEGF-ir was in round nucleus cells scattered around biomaterial particles and inside the degrading biomaterial as well. The Figure 16 show the percentage area of VEGF-ir in each group. In both groups, positive VEGF expression was also observed in blood vessels, extracellular matrix and bone cells. However, an increased number of osteocytes immunostained for VEGF.

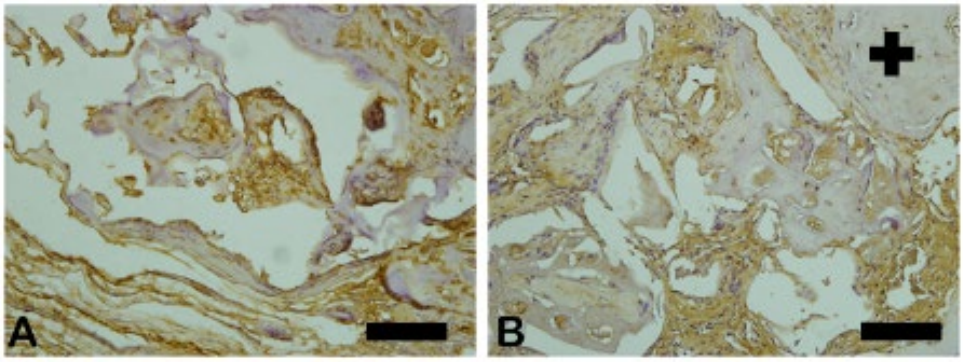

Figure 15. - VEGF-stained photomicrographs. The brownish deposits indicate VEGF's presence and its activity, which is involved in the process of the formation of new blood vessels. (A) Autogenous bone group, (B) n-HA/β-TCP group. Scale bar 100 μm, ×200 magnification.

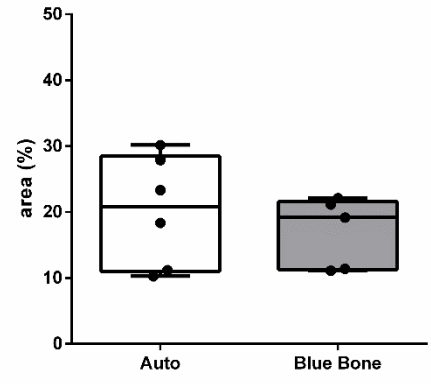

Figure 16. - Result of the histomorphometric analysis of immunostaining to VEGF: Autogenous bone group and n-HA/β-TCP composite group. * p = 0.6277.

 doi:10.20944/preprints202410.1932.v1

3.8NFκ-β (Nuclear Factor Kappa-Beta)

The NFκ-β regulates TNF-α and RANK-L, hence, inducing osteoclasts differentiation (Figure 17). The Figure 18 shows the percentage of area of NFκ-β in each group. In the immunohistochemistry for Nuclear Factor kappa B (NFKB) in the Figure 17A indicated by the arrow we can see the immunolabeling exactly in an osteoclast. In the Figure 17B we can see immunolabeled islands showing the regulation of osteoclasts.

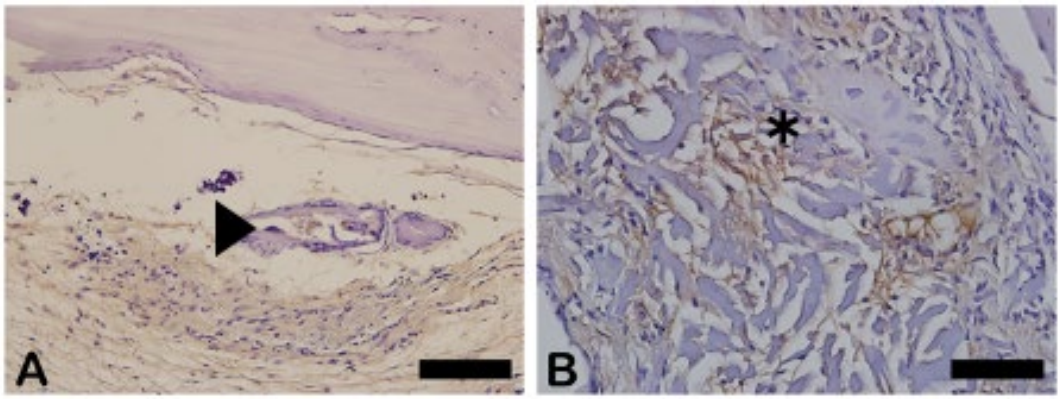

Figure Immunohistochemical labeling for Nuclear Factor kappa B (NFKB). (A) Expression NFKB was visualized slight in extracellular matrix and osteoclast (arrowhead). (B) The little more intense staining was observed in extracellular matrix and fibroblasts-like cells (asterisk).

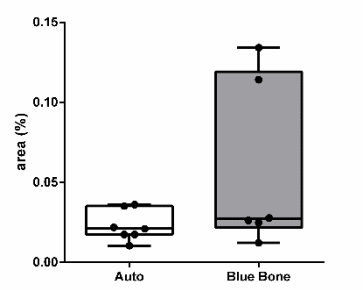

Figure 18. - Result of the histomorphometric analysis of immunostaining to NFκ-β: Autogenous bone group and n-HA/β-TCP composite group. * p = 0.2191.

3.9. Metalloproteinase-9 (MMP-9)

The MMP-9 was observed in dark brown deposits inside osteoblasts and in bone matrix (Figure 19). Decreased MMP-9 can influence the bending strength and toughness bone because affect ECM proteins. In B group was noted most intense staining in extracellular matrix, osteocytes (cross) and fibroblasts-like cells showing more influence bone strength. The Figure 20 shows the area percentage of MMP-9 in the samples, suggesting a expressive higher of MMP-9 in Blue Bone group.

 doi:10.20944/preprints202410.1932.v1

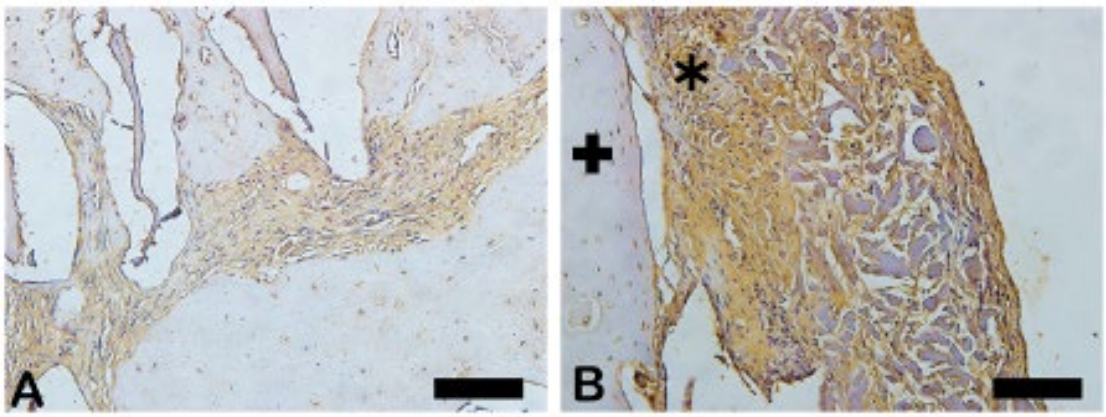

Figure 19. - Immunohistochemical labeling for Metaloproteinases-9. (A) Expression MMP-9 was visualized slight in extracellular matrix. (B) The strong marking staining was observed in extracellular matrix (asterisk). In both groups, osteocytes (cross) and fibroblast-like cells were also immunostained being more intense in group B. Scale bar = 100 μm, x200 magnification.

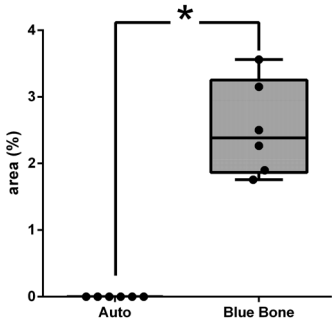

Figure 20. - Result of the histomorphometry analysis of immunostaining to MMP-9: Autogenous bone group and n-HA/β-TCP composite group. * p = 0.0022.

3.10. MMP-2 (Metalloproteinase-2)

The dark brown deposits indicate MMP-2-ir in osteoblasts and bone matrix (Figure 21).

The MMP-2 MMP-2 is a gelatinase related with bone integrity because those deficiency affect mineral ion exchanges occur during the resorption and mineralization of the bone matrix. In B group was noted most intense staining in extracellular matrix, osteocytes and fibroblasts-like cells showing more potential in maintaining bone mineral density**.** [32] (Figure 21) The Figure 22 shows the area percentage of MMP-2 in the samples, suggesting a higher amount of enzyme content.

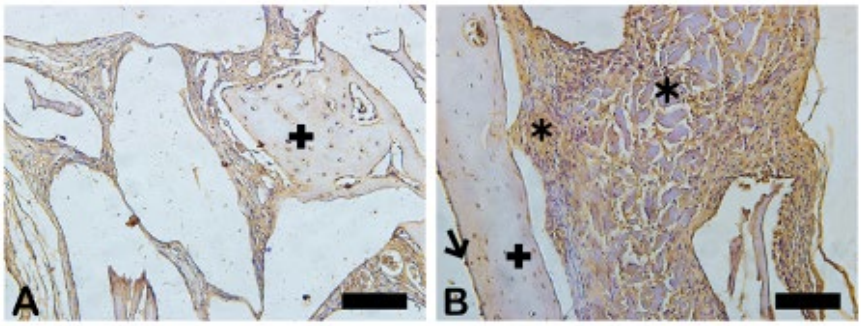

Figure 21. - Immunohistochemical labeling for Metalloproteinases 2. (A) Expression MMP-2 were visualized slight in extracellular matrix and in several osteocytes (cross). (B) The strong marking was

 doi:10.20944/preprints202410.1932.v1

observed in extracellular matrix, osteoblasts (arrow), osteocytes (cross) and fibroblasts-like cells (asterisk). Scale bar = 100 μm, x200 magnification.

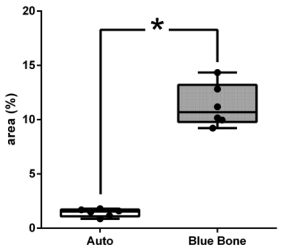

Figure 22. - Result of the histomorphometric analysis of immunostaining to MMP-2: Autogenous bone group and n-HA/β-TCP composite group. * p = 0.0025.

3.11. Schiff's Periodic Acid (PAS)

The PAS method is based on Schiff's periodic acid oxidizing hydroxyl and amino/alkyl amine chemical groups, forming a magenta-colored complex. It detected polysaccharides, glycoproteins, and glycolipids, suggesting new bone formation (Figure 23).

The PAS presents a positive reaction with mineralized bone while it does not react with osteoid tissue. [33] The results showed thick PAS positive trabeculae in the Blue Bone group (REG) and a single thin trabecula in the Autogenous group (arrows) suggesting the osteogenic potential of the Blue Bone group (REG). (Figure 24)

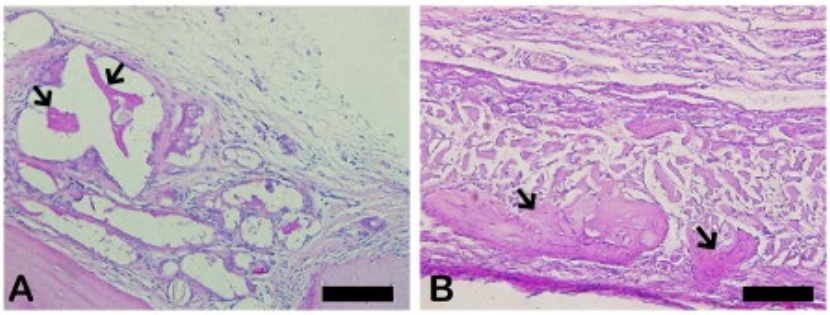

Figure 23. - Photomicrographs of critical defect slides stained with periodic acid-Schiff-(PAS-) showing positive reaction for calcified bone (pink) and negative reaction for osteoid tissue. (A) Thin trabeculae of mineralized bone are visualized in Autogenous group. (B) Thick trabeculae of mineralized bone are observed in Blue Bone group (REG). Scale bar 100 μm, ×200 magnification.

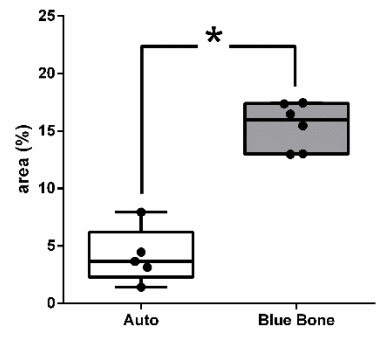

Figure 24. - Result of the histomorphometric analysis of PAS histochemistry: Autogenous bone group and n-HA/β-TCP composite group. * p = 0.0043.

 doi:10.20944/preprints202410.1932.v1

3.12. Bone Morphogenic Proteins-2 (BMP-2)

The BMP-2 is an extremely important signal in the process of bone remodeling because it regulates the differentiation of mesenchymal cells into osteoblasts, maintaining the stability of the process. The asterisks show the regions of darker brown that are considered to be intense markings revealing the presence of osteoblasts and osteoid matrix. (Figure 25)

The *Mann Whitney test* showed that no significant statistical relevance was found in the Blue Bone group in relation to the Auto group. (Figure 26)

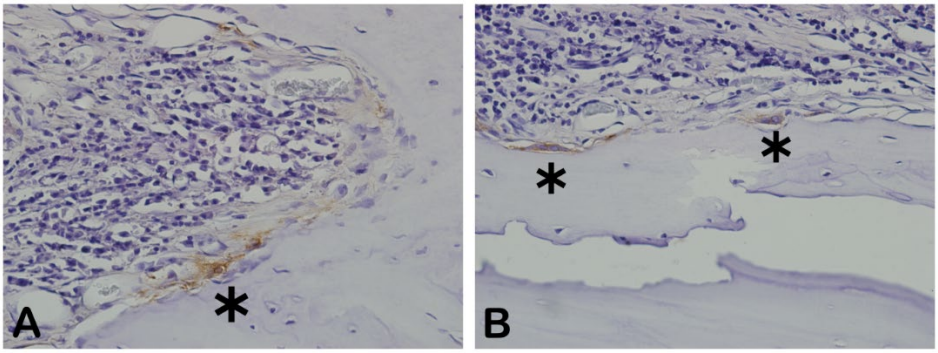

Figure 25. - Photomicrographs of metalloproteinase (BMP-2) stained slides. Brown color indicates osteoblastic activity. (**A**) Group 1 (Blue Bone), (**B**) Group 2 (autogenous). Scale bar = 100 μm, 20× magnification.

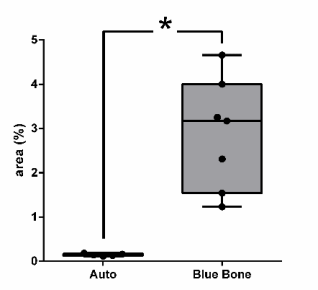

Figure 26. - Result of the histomorphometric analysis int the inflammation regulation through osteoblast activity by BMP-2: Autogenous group and Blue Bone group (REG). * $p < 0.0001$.

3.13. Real-Time Polimerase Chain Reaction (RT-qPCR)

The RT-qPCR data on *RANKL* gene expression indicates no difference between groups. On the other hand, *OSTEOCALCIN*, *ALKALINE PHOSPHATASE*, *OSTERIX* and *RUNX2* showed a significant reduction on gene expression in n-HA/β-TCP group (Figure 27).

 doi:10.20944/preprints202410.1932.v1

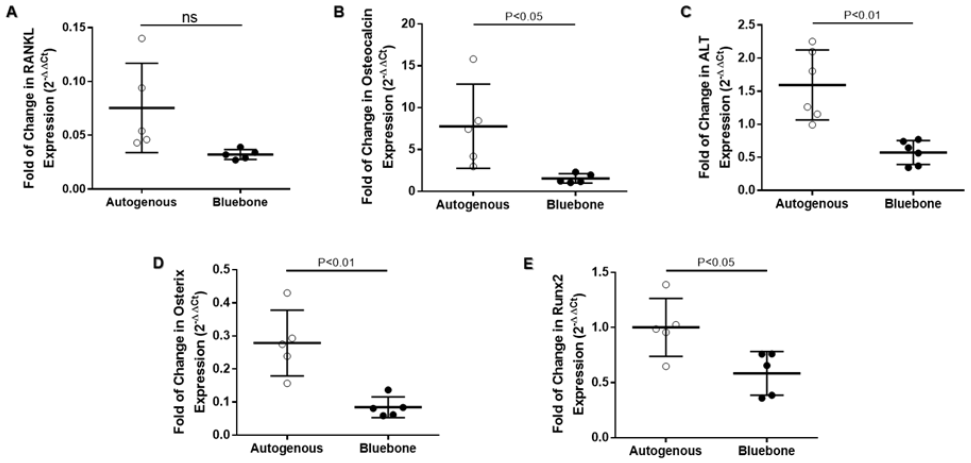

Figure 27. - Expression analysis of *RANKL* (A), *OSTEOCALCIN* (B), *ALP* (C), *OSTERIX* (D) and *RUNX2* (E) in calvaria of rats with two types of bone grafts (Autogenous and Blue bone™) 60 days after induced injury. The results represent the fold of chance of each mRNA expression upon the control and it is expressed by the mean of 5 animals per group and ⌾ SD. To statistical analysis, values was submitted to parametric unpaired t-test with Welch's correction and P<0.05 between groups was considered significant. Legend: Receptor activator of nuclear factor- κB ligand (RANKL); Alkaline phosphatase (ALP); Runt-related transcription factor 2 (Runx2).

3.14. Validation Test to Analysis of Acid Phosphatase (AP) Activity in Bone

The validation of AP assay kit shows it to be possible to evaluate acid phosphatase activity (Figure 28A) and non-TRAP activity (Figure 28B) in plasma, as well as in the rats' bone tissue. Although the AP activity shows to be significantly decreased in bone (0.0034⌾0.002608) when compared to plasma (0.0108⌾0.002775), those results are probably caused by the difference in the amount of protein of each sample. The non-Tartrate Resistant Acid Phosphatase activity (non-TRAP activity) shows no significant difference between plasma and bone, indicating that the amount of AP derived from osteoclast is similar in both plasma (0.00454⌾0.003627) and bone (0.00158⌾0.001117).

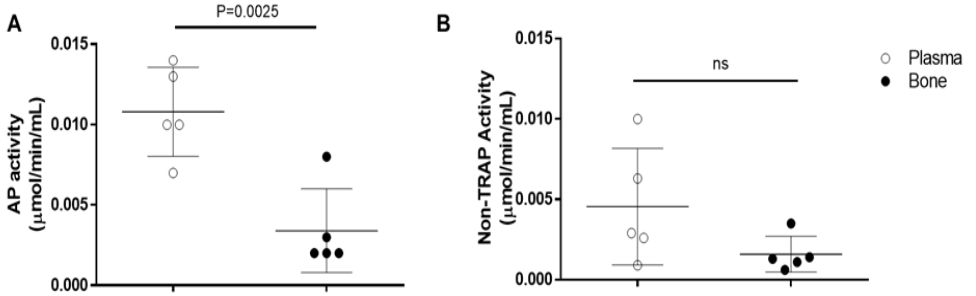

Figure 28. - Validation of Bone-derived Acid Phosphatase Activity. To validate the Acid Phosphatase Colorimetric Assay Kit (# 10008051, Cayman Chemical/ Michigan, USA) we used 20⌾L of plasma and bone-extracted supernatant as described in the datasheet. (**A**) Analysis of total acid phosphatase activity; (**B**) Analysis of Non-Tartrate Resistant Acid Phosphatase activity. Groups are represented by mean⌾SD. Statistics were carried out with One-Way (ANOVA) with post-test of Holm-Sidak.

3.15. Acid Phosphatase Assay

In both AP activity (Figure 29A) and non-TRAP activity (Figure 29B) no difference was observed between acid phosphatase derived from bones control group (0.0590⌾0.03851; 0.0288⌾0.01968) and the group grafted with autogenous bone (0.0662⌾0.01465; 0.0332⌾0.006979). The group grafted with

 doi:10.20944/preprints202410.1932.v1

n-HA/β-TCP presented a significant increasing of AP activity (0.2074⊚0.09938) and non-TRAP activity (0.1018⊚0.04779) compared to control group and the group grafted with autogenous bone. Although the non-TRAP activity is similar to 50% of total AP activity, those results suggest an increased remodeling of the bone by activation of the osteoclasts.

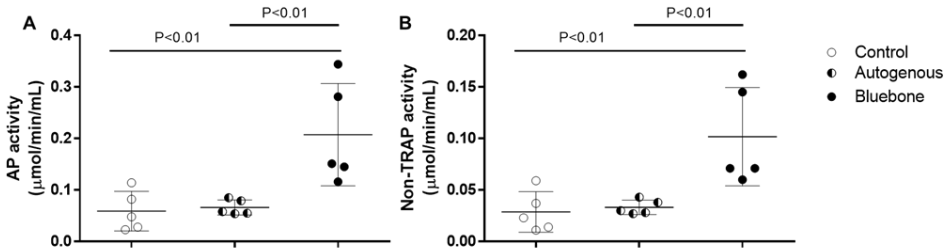

Figure 29. - Analysis of Bone-derived Acid Phosphatase (AP) activity in calvaria of rats grafting with autogenous bone ( ) or blue bone ( ). (**A**) Analysis of total acid ( ) phosphatase.( )activity; (**B**) Analysis of Non-Tartrate Resistant Acid Phosphatase activity. Groups are represented by mean⊚SD. Statistic was accessed by One-Way (ANOVA) with post-test of Holm-Sidak.

3.16. MEV (Scanning Electron Microscopy)

Figure 30 shows the SEM images, it is possible to observe structures related to bone remodeling process, like bone matrix trabeculae, biopolymers, in addition to osteoblasts and osteoclasts.

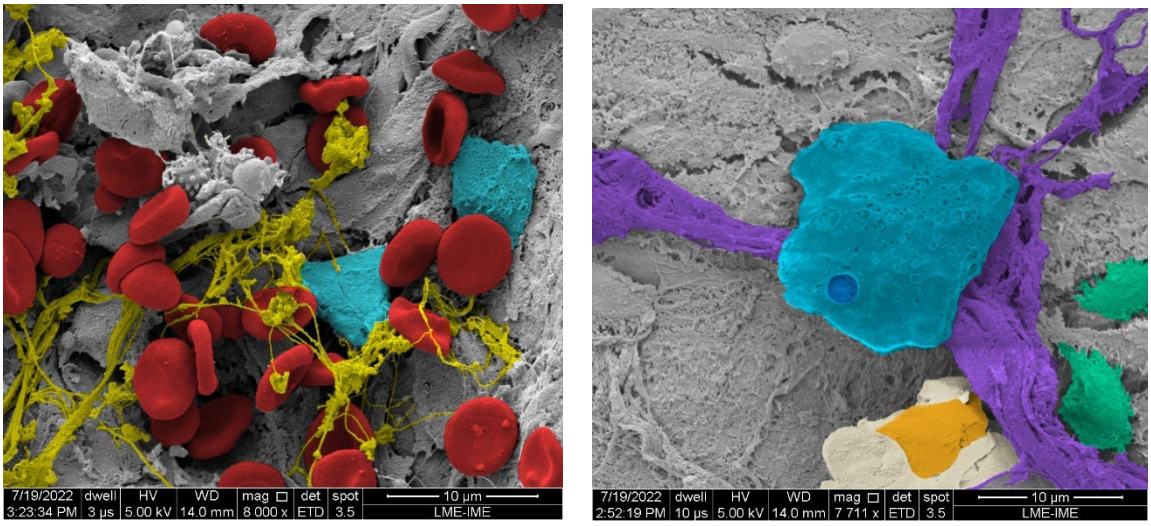

Figure 30. - Scanning electron micrographs, (A) The autogenous graft group, showing red blood cells (red) collagen fibrils (yellow) and endothelial cells (light blue). x8000 magnification. (B) The n-HA/β-TCP composite group, showing the biomaterial particle (light blue), collagen fibers (purple), osteoblast (Orange) and osteocytes inside lacunae (green). x7711 magnification.

4. Discussion

The bone tissue morpho-physiology and response to trauma and disease is a flourishing field of research. It received additional importance to support the design and manufacturing of graft biomaterials, [34].

In this study we provided morpho-physiological evidence that a synthetic biomaterial has the potential to enhance more natural responses to trauma than autogenous bone. In our comparison between a synthetic biomaterial (n-HA/ß-TCP composite) and autogenous grafts it was found that: (1) in histomorphometric evaluation (Goldner's Trichromic, Periodic Acid-Schiff, Tartrate Resistant Acid Phosphatase, Picrosirius Red) the n-HA/ß-TCP composite presented more new bone formation area than autogenous bone; (2) In phosphatase alkaline assay the n-HA/ß-TCP composite showed

 doi:10.20944/preprints202410.1932.v1

higher activity than autogenous bone; (3) in immunohistochemistry evaluation (Cathepsin K, TGF-β, Osteopontin, VEGF, NFκ-β, MMP-2, MMP-9) the n-HA/ß-TCP composite presented more immunoreactive area than autogenous bone. On the other hand, the in Rt-PCR analysis (*OSTEOCALCIN*, *ALKALINE PHOSPHATASE*, *OSTERIX* and *RUNX2*) showed a higher gene expression on autogenous bone group, but *RANKL* gene expression. (Figure 27)

Goldner's Masson staining is considered one of the best staining techniques to distinguish between new bone matrix and mature bone matrix. [35] Picrosirius red staining is more focused on identification of fibrillar collagen networks. [36] Additionally, Periodic Acid-Shiff is the choice staining method to detect polysaccharides, glycoproteins, and glycolipids in bone matrix. [37] Took together, the more extensive bone matrix production in n-HA/ß-TCP composite group, suggests a faster production of the organic matrix component than autogenous bone group. The MEV photomicrographs highlights collagen bundles and fibrils in n-HA/ß-TCP composite group.

Acid phosphatase (AP) induces inorganic phosphate release from the mineralization inhibitor inorganic pyrophosphate (PPi) in bone matrix. The Tartarate-resistent acid phosphatase (TRAP) exhibits potent phosphatase activity on Osteopontin (OPN) and its dephosphorylation reduces OPN inhibitory mineralization potential. [38–40]**.**

In spite of founding a higher immunireativity of OPN, higher activities were found of Acid phosphatese (AP) and Tartarate-resistent acid phosphatase (TRAP) in n-HA/ß-TCP composite group, indicating a greater mineralization potential, according to Linder et al [39] proposal.

Cathtepsin K is mainly found in osteoclasts, the bone cell type related to bone matrix absorbing and its gene expression is regulated by RANKL-RANK transduction signal (NFκ-β). Cathtepsin K is highly efficient to break down type I collagen and osteonectin that comprise most of the organic bone matrix. Additionally, it is able to activate (by cleaving) matrix-metalloproteinase-9 (MMP-9), that contributes to bone matrix degradation as well. [41]

It was found a significant higher Cathepsin K and MMP-9-immunoreactivity in n-HA/ß-TCP composite group. However, no difference was found in NFκ-β-immunoreactivity, nor *RAMKL* RT-qPCR between the groups. These data suggest a higher bone matrix turnover in n-HA/ß-TCP composite group**.** [42]

The Transforming Growth Factor-β (TGF-β) is superfamily that comprises the bone morphogenetic proteins (BMP) and TGF-β1) are known to act locally on bone formation, by stimulating the proliferation and chondrogenic/osteogenic differentiation of mesenchymal stem cells (MSCs). However, the TGF-β family is able to induce osteoclastogenesis and matrix resorption activity. Additionally, it can sustain mature osteoclasts survival directedly by way of osteoblast-osteocytes modulation. In this respect, the TGF-β superfamily has a center role in orchestrate the bone matrix formation and resorption in bone remodeling. [22–43] We found a higher TGF-β-immunireactivity in n-HA/ß-TCP composite group, suggesting a higher rate of remodeling in this group.

In addition to the matrix-metalloproteinase-9 (MMP-9), the matrix-metalloproteinase-2 (MMP-2) is an important player in organic bone matrix resorption. However, some distinct characteristics are unique to MMP-2: it is related to osteocyte surviving and canalicular maintaining, osteogenic differentiation, in addition to osteoblasts and osteoclasts surviving. [44,45]**.** We found a higher MMP-2-immunoreaction in n-HA/ß-TCP composite group, suggesting a more sustained bone remodeling than autogenous bone group.

The Vascular Endothelial Growth Factor (VEGF) is one of the most powerful inducers of angiogenesis and it plays critical roles in bone development/remodeling. [46] Our data indicates a higher VEGF-immunoreactivity in n-HA/ß-TCP composite group, suggesting an enhanced potential for bone remodeling.

The RUNX2 and OSX are the transcription factors more important to the induction of the Mesenchymal Stem Cells (MSCs) to differentiate towards the osteogenic lineage. [22–48] Our RT-qPCR data indicates a higher RNAm expression of RUNX2 and OSX in addition to *ALKALINE PHOSPHATASE*, in the autogenous bone group.

 doi:10.20944/preprints202410.1932.v1

Osteocalcin (OCN) is a non-collagenous protein secreted by osteoblasts that is able to be stored in the bone matrix due to its capability to bind to hydroxyapatite. The OCN can be activated by two different processes: via osteoclasts or acid pH. It is believed that OCN inhibits bone formation and induces hydroxyapatite crystals parallel aligning to the collagen bundles. [49,50] Our data indicates a higher OCN gene expression in autogenous bone group.

Figure 31 summarizes the hypothetical bone remodeling mechanisms from the data found in this work.

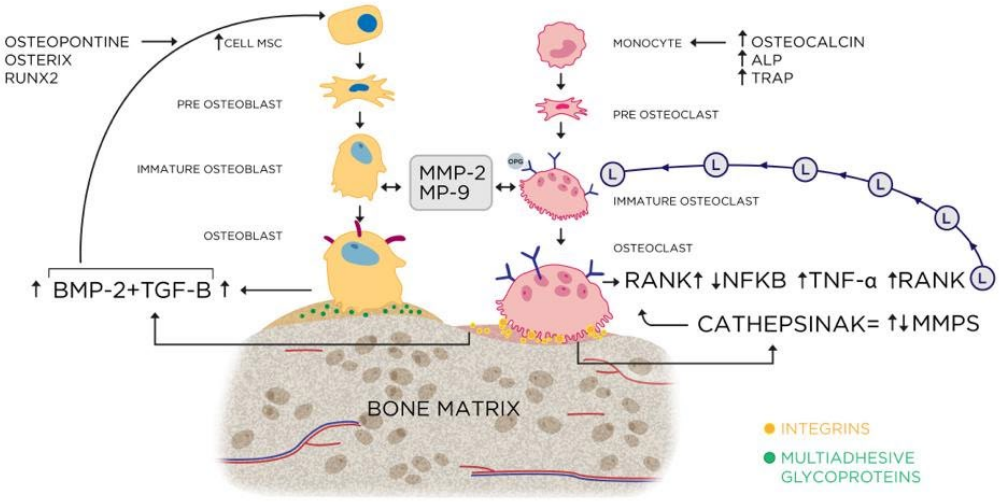

Figure 31. - Representative scheme of the activation cascade of the bone remodeling process, involving the markers present in this study.

The overall panorama achieved in this experiment indicates that n-HA/ß-TCP composite group presented significant gains in most substances tested, including traditional staining methods. On the other hand, most of the RNAm tested were higher in autogenous bone group. It is worth to remark that RNAm presence is a prediction of near future cellular events if traduction effectively takes place**.** [51]

Synthetic biomaterials design, production and testing is a fast growing and promising field of research. As technologies evolves the closer biomaterials properties get to native bone, eventually mimicking it and maybe surpassing it. If corroborated and extended by future experiments and by other research groups, the data presented in this work could be a relevant mark in synthetic biomaterial research.

5.Conclusions

Based on the presented results, we can affirm that the nano-hydroxyapatite influenced a more effective osteoinduction than the autogenous bone, indicating that that.

1- Nanogeometry creates a more favorable structure for cell adhesion and development.

2- There was an intense formation of bone matrix in Goldener's Trichrome staining, PAS and PSR.

3- In immunohistochemistry, there was a prevalence of cells such as osteoblasts and osteoclasts for nanohydroxyapatite, in addition to several potentially more abundant blood vessels when analyzed with VEGF.

4- The rt-PCR test and Elisa test also confirmed results shown in the previous tests, demonstrating a significantly more favorable response for the bone maturation process in the case of the nano-hydroxyapatite/beta-tricalcium phosphate composite**.** nanohydroxyapatite.

5- In the ultrastructural analysis, it was possible to describe that in the same period, bone physiology was better defined and structured in nanohydroxyapatite than in autogenous bone.

Future Perspectives

In vitro analysis should provide additional biochemical data to a more detailed understanding of the naïve bone-biomaterial interactions and possibly improve further biomaterial design.

Authors' contributions: Igor Brum: Conceptualization, Data curation, **Lucio Frigo:** Writing - Original Draft, Writing - Review & Editing, **Jemima Ribeiro:** Investigation, **Bianca Torres:** Investigation, **Ana Lucia:** Investigation, **Mario José:** Formal analysis, **Carlos Nelson:** Methodology, **Jorge José:** Supervision.

References

1. [1] Archunan M W, Petronis S (September 04, 2021) Bone Grafts in Trauma and Orthopaedics 2021 *Cureus* **13(9)** eDOI 10.7759/cureus.17705
2. [2] Bone Grafts And Substitutes Market Size, Share & Trends Analysis Report By Material Type (Allograft, Synthetic), By Application (Spinal Fusion, Foot & Ankle, Joint Reconstruction), By Region, And Segment Forecasts, 2022 – 203 https://www.grandviewresearch.com/industry-analysis/bone-grafts-substitutes-market. Accessed in 05. 05. 2023
3. [3] Veronesi, F, Maglio, M, Brogini, S, Fini, M. In vivo studies on osteoinduction: A systematic review on animal models, implant site, and type and postimplantation investigation 2020 *J Biomed Mater Res*. **108** 1834– 1866. https://doi.org/10.1002/jbm.a.36949
4. [4] Steijvers, E.; Ghei, A.; Xia, Z. Manufacturing artificial bone allografts: a perspective. 2022 *Biomater Transl* **3(1)** 65-80. http://doi.org/10.12336/ biomatertransl.2022.01.007
5. [5] Wang T, Yang X, Qi X, Jiang C. Osteoinduction and proliferation of bone-marrow stromal cells in three-dimensional poly (ε-caprolactone)/ hydroxyapatite/collagen scaffolds. 2015 *J Transl Med* May **8;13** 152. doi: 10.1186/s12967-015-0499-8.
6. [6] Weber FE. Reconsidering Osteoconduction in the Era of Additive Manufacturing. 2019 *Tissue Eng Part B Rev* **25(5)** 375-386. doi: 10.1089/ten.TEB.2019.0047.
7. [7] Tansavatdi K, Mangat DS. Calcium hydroxyapatite fillers. 2011 *Facial Plast Surg* **27(6)** 510-516. doi: 10.1055/s-0031-1298783.
8. [8] Liu YJ, Yang ZY, Tan LL, Li H, Zhang YZ. An animal experimental study of porous magnesium scaffold degradation and osteogenesis. 2014 *Braz J Med Biol Res* **47(8)** 715-720. doi: 10.1590/1414-431x20144009.
9. [9] Paulo MJE, Dos Santos MA, Cimatti B, Gava NF, Riberto M, Engel EE. Osteointegration of porous absorbable bone substitutes: A systematic review of the literature. 2017 *Clinics* **72(7)** 449-453. doi: 10.6061/clinics/2017(07)10.
10. [10] Xu Y, Shao B, Zeng X, Song Z, Jia M, Gong Z. Biofunctional Extracellular Matrix-Polycaprolactone-Hydroxyapatite Scaffold and Synovium Mesenchymal Stem Cells/Chondrocytes for Repairing Cartilage Defects. 2021 *Tissue Eng* **27(19-20)** 1250-1263. doi: 10.1089/ten.TEA.2020.0245.
11. [11] Yang Y, Lin H, Shen H, Wang B, Lei G, Tuan RS. Mesenchymal stem cell-derived extracellular matrix enhances chondrogenic phenotype of and cartilage formation by encapsulated chondrocytes in vitro and in vivo. 2018 *Acta Biomater* **15;69** 71-82. doi: 10.1016/j.actbio.2017.12.043.
12. [12] Corduff N. Introducing aesthetic regenerative scaffolds: An immunological perspective. 2023 *J Cosmet Dermatol* **22 Suppl** 8-14. doi: 10.1111/jocd.15702.
13. [13] Fitzpatrick V, Martín-Moldes Z, Deck A, Torres-Sanchez R, Valat A, Cairns D, Li C, Kaplan DL. Functionalized 3D-printed silk-hydroxyapatite scaffolds for enhanced bone regeneration with innervation and vascularization. 2021 *Biomaterials* **276** 120995. doi: 10.1016/j.biomaterials.2021.120995.
14. [14] Chen S, Shi Y, Zhang X, Ma J. Evaluation of BMP-2 and VEGF loaded 3D printed hydroxyapatite composite scaffolds with enhanced osteogenic capacity in vitro and in vivo. 2020 *Mater Sci Eng C Mater Biol Appl* **112** 110893. doi: 10.1016/j.msec.2020.110893.
15. [15] Sritharan S, Kannan TP, Norazmi MN, Nurul AA. The synergistic effects of IL-6/IL-17A promote osteogenic differentiation by improving OPG/RANKL ratio and adhesion of MC3T3-E1 cells on hydroxyapatite. 2018 *J Craniomaxillofac Surg* **46(8)** 1361-1367. doi: 10.1016/j.jcms.2018.05.002.
16. [16] Talal A, McKay IJ, Tanner KE, Hughes FJ. Effects of hydroxyapatite and PDGF concentrations on osteoblast growth in a nanohydroxyapatite-polylactic acid composite for guided tissue regeneration. 2013 *J Mater Sci Mater Med* **24(9)** 2211-2221. doi: 10.1007/s10856-013-4963-9.
17. [17] Jakobsen SS, Larsen A, Stoltenberg M, Bruun JM, Soballe K. Hydroxyapatite coatings did not increase TGF-beta and BMP-2 secretion in murine J774A.1 macrophages but induced a pro-inflammatory cytokine response. 2009 *J Biomater Sci Polym Ed* **20(4)** 455-465. doi: 10.1163/156856209X416476.
18. [18] Binatti E, Zoccatelli G, Zanoni F, Donà G, Mainente F, Chignola R. Phagocytosis of Astaxanthin-Loaded Microparticles Modulates TGFβ Production and Intracellular ROS Levels in J774A.1 Macrophages. 2021 *Mar Drugs* **19(3)** 163. doi: 10.3390/md19030163.
19. [19] Guo P, Liu X, Zhang P, He Z, Li Z, Alini M, Richards RG, Grad S, Stoddart MJ, Zhou G, Zou X, Chan D, Tian W, Chen D, Gao M, Zhou Z, Liu S. A single-cell transcriptome of mesenchymal stromal cells to

fabricate bioactive hydroxyapatite materials for bone regeneration. 2021 *Bioact Mater* Aug **11;9** 281-298. doi: 10.1016/j.bioactmat.2021.08.009.

20. [20] Manzini, B.M., Machado, L.M.R., Noritomi, P.Y. *et al.* Advances in Bone tissue engineering: A fundamental review. 2021 *J Biosci* **46** 17. https://doi.org/10.1007/s12038-020-00122-6.
21. [21] Ralston SH, Bone structure and metabolism, 2017 *Medicine* **45;9** 560-564 http://dx.doi.org/10.1016/j.mpmed.2017.06.008.
22. [22] Salhotra, A., Shah, H.N., Levi, B. *et al.* Mechanisms of bone development and repair. 2020 *Nat Rev Mol Cell Biol* **21** 696–711. https://doi.org/10.1038/s41580-020-00279-w
23. [23] Proff P, Römer P. The molecular mechanism behind bone remodelling: a review. 2009 *Clin Oral Investig* **13(4)** 355-362. doi: 10.1007/s00784-009-0268-2.
24. [24] Eriksen, E.F. Cellular mechanisms of bone remodeling. 2010 *Rev Endocr Metab Disord* **11** 219–227. https://doi.org/10.1007/s11154-010-9153-1
25. [25] Allori AC, Sailon AM, Warren SM. Biological basis of bone formation, remodeling, and repair-part I: biochemical signaling molecules. 2008 *Tissue Eng Part B Rev* **14(3)** 259-273. doi: 10.1089/ten.teb.2008.0082.
26. [26] Filip DG, Surdu VA, Paduraru AV, Andronescu E. Current Development in Biomaterials-Hydroxyapatite and Bioglass for Applications in Biomedical Field: A Review. 2022 *J Funct Biomater* **16;13(4)** 248. doi: 10.3390/jfb13040248.
27. [27] Wang C, Liao H, Cao Z. Role of Osterix and MicroRNAs in Bone Formation and Tooth Development. 2016 *Med Sci Monit* **20;22** 2934-2942. doi: 10.12659/msm.896742.
28. [28] Guo L, Xin H, Luo X, Zhang C. Phase evolution, mechanical properties and MRI contrast behavior of $GdPO_4$ doped hydroxyapatite for dental applications. 2020 *Mater Biol Appl* **111** 110858. doi: 10.1016/j.msec.2020.110858.
29. [29] Lu, Jingyi et al. "Biological properties of calcium phosphate biomaterials for bone repair: a review. 2018 *RSC Advances* **8** 2015-2033.
30. [30] Li Q, Feng C, Cao Q, Wang W, Ma Z, Wu Y, He T, Jing Y, Tan W, Liao T, Xing J, Li X, Wang Y, Xiao Y, Zhu X, Zhang X. Strategies of strengthening mechanical properties in the osteoinductive calcium phosphate bioceramics. 2023 *Regen Biomater* **17;10** rbad013. doi: 10.1093/rb/rbad013.
31. [31] Dayan D, Hiss Y, Hirshberg A, Bubis JJ, Wolman M. Are the polarization colors of picrosirius red-stained collagen determined only by the diameter of the fibers? 1989 *Histochemistry* **93(1)** 27-9. doi: 10.1007/BF00266843.
32. [32] Liang HPH, Xu J, Xue M, Jackson CJ. Matrix metalloproteinases in bone development and pathology: current knowledge and potential clinical utility. 2016 *Metalloproteinases In Medicine* **3** 93-102, https://doi.org/10.2147/MNM.S92187.
33. [33] Raina V. Normal osteoid tissue. 1972 *J Clin Pathol* **25(3)** 229-32. doi: 10.1136/jcp.25.3.PMID: 4111820; PMCID: PMC477268.
34. [34] Ribeiro LA, Magalhães HIR, Silva AF, Silva FOCE. Macroscopic, morphometric, and tomographic features of the mandible of the collared peccary (Pecari tajacu) applied to clinical morpho-physiology and imaging. 2022 *Anat Rec (Hoboken)* **305(11)** 3178-3191. doi: 10.1002/ar.24897.
35. [35] Gruber HE. Adaptations of Goldner's Masson trichrome stain for the study of undecalcified plastic embedded bone. 1992 *Biotech Histochem* **67(1)** 30-4. doi: 10.3109/10520299209110002.
36. [36] Lattouf R, Younes R, Lutomski D, Naaman N, Godeau G, Senni K, Changotade S. Picrosirius red staining: a useful tool to appraise collagen networks in normal and pathological tissues. 2014 *J Histochem Cytochem* **62(10)** 751-758. doi: 10.1369/0022155414545787.
37. [37] Kjosness, K.M., Reno, P.L. and Serrat, M.A. Modified Periodic Acid-Schiff (PAS) Is an Alternative to Safranin O for Discriminating Bone–Cartilage Interfaces. 2023 *JBMR Plus* **7** e10742. https://doi.org/10.1002/jbm4.10742.
38. [38] Sharma U, Pal D, Prasad R. Alkaline phosphatase: an overview. 2014 *Indian J Clin Biochem* **29(3)** 269-78. doi: 10.1007/s12291-013-0408-y.
39. [39] Halling Linder C, Ek-Rylander B, Krumpel M, Norgård M, Narisawa S, Millán JL, Andersson G, Magnusson P. Bone Alkaline Phosphatase and Tartrate-Resistant Acid Phosphatase: Potential Co-regulators of Bone Mineralization. 2017 *Calcif Tissue Int* **101(1)** 92-101. doi: 10.1007/s00223-017-0259-2.
40. [40] Vimalraj S. Alkaline phosphatase: Structure, expression and its function in bone mineralization. 2020 *Gene* **5;754** 144855. doi: 10.1016/j.gene.2020.144855.
41. [41] Dai R, Wu Z, Chu HY, Lu J, Lyu A, Liu J and Zhang G. Cathepsin K: The Action in and Beyond Bone. 2020 *Front Cell Dev Biol* **8** 433. doi: 10.3389/fcell.2020.00433.
42. [42] Kumar A, Mahendra J, Mahendra L, Abdulkarim HH, Sayed M, Mugri MH, Ahmad ZH, Bhati AK, Faqehi HH, Algregri WO, Varadarajan S, Balaji TM, Baeshen HA, Patil S. Synergistic Effect of Biphasic Calcium Phosphate and Platelet-Rich Fibrin Attenuate Markers for Inflammation and Osteoclast Differentiation by Suppressing *NF-κB/MAPK* Signaling Pathway in Chronic Periodontitis. 2021 *Molecules* **30;26(21)** 6578. doi: 10.3390/molecules26216578.

43. [43] Jann J, Gascon S, Roux S, Faucheux N. Influence of the TGF-β Superfamily on Osteoclasts/Osteoblasts Balance in Physiological and Pathological Bone Conditions. 2020 *Int J Mol Sci* **14;21(20)** 7597. doi: 10.3390/ijms21207597.
44. [44] Paiva KBS, Granjeiro JM. Matrix Metalloproteinases in Bone Resorption, Remodeling, and Repair. 2017 *Prog Mol Biol Transl Sci* **148** 203-303. doi: 10.1016/bs.pmbts.2017.05.001.
45. [45] Lieu S, Hansen E, Dedini R, Behonick D, Werb Z, Miclau T, Marcucio R, Colnot C. Impaired remodeling phase of fracture repair in the absence of matrix metalloproteinase-2. 2011 *Dis Model Mech* **4(2)** 203-211. doi: 10.1242/dmm.Epub 2010 Dec PMID: 21135056; PMCID: PMC3046093.
46. [46] Hu K, Olsen BR. The roles of vascular endothelial growth factor in bone repair and regeneration. 2016 *Bone* **91** 30-8. doi: 10.1016/j.bone.2016.06.Epub 2016 Jun PMID: 27353702; PMCID: PMC4996701.
47. [47] Chan WCW, Tan Z, To MKT, Chan D. Regulation and Role of Transcription Factors in Osteogenesis. 2021 *Int J Mol Sci* May **21;22(11)** 5445. doi: 10.3390/ijms22115445.
48. [48] Narayanan A, Srinaath N, Rohini M, Selvamurugan N. Regulation of Runx2 by MicroRNAs in osteoblast differentiation. 2019 *Life Sci* **1;232** 116676. doi: 10.1016/j.lfs.2019.116676.
49. [49] Rossi M, Battafarano G, Pepe J, Minisola S, Del Fattore A. The Endocrine Function of Osteocalcin Regulated by Bone Resorption: A Lesson from Reduced and Increased Bone Mass Diseases. 2019 *Int J Mol Sci* Sep **11;20(18)** 4502. doi: 10.3390/ijmsPMID: 31514440; PMCID: PMC6769834.
50. [50] Komori T. Functions of Osteocalcin in Bone, Pancreas, Testis, and Muscle. 2020 *Int J Mol Sci* **12;21(20)** 7513. doi: 10.3390/ijms21207513.
51. [51] Leng Q, Chen L, Lv Y. RNA-based scaffolds for bone regeneration: application and mechanisms of mRNA, miRNA and siRNA. 2020 *Theranostics* **10;10(7)** 3190-3205. doi: 10.7150/thno.PMID: 32194862; PMCID: PMC7053199.